SSC19-VI-04

Optical Communications Crosslink Payload Prototype Development for the Cubesat Laser Infrared CrosslinK (CLICK) Mission

Paul Serra, Ondrej Cierny, Rodrigo Diez, Peter Grenfell, Grant Gunnison, Will Kammerer, Joe Kusters
Cadence Payne, Joseph Murphy, Tao Sevigny, Paula do Vale Pereira, Laura Yenchesky
Kerri Cahoy
Massachusetts Institute of Technology
77 Massachusetts Avenue, Cambridge, MA 02139; +1-617-253-7805
pserra@mit.edu, kcahoy@mit.edu

Myles Clark, Tyler Ritz, Danielle Coogan, John Conklin
University of Florida
231 MAE-A, P.O. Box 116250, Gainesville, FL 32611-6250; +1-352-392-0614
jwconklin@ufl.edu

David Mayer, John Hanson, Jan Stupl
NASA Ames Research Center
Moffett Field, CA, 94035
david.j.mayer@nasa.gov

ABSTRACT

The Cubesat Laser Infrared CrosslinK (CLICK) mission is a technology demonstration of <1.5U nanosatellite laser communications terminals, with downlinks from low-Earth orbit altitudes of 400-600 km to a portable optical ground station, and crosslinks over ranges from 25-580 km. The mission has two separate launches and three total 3U CubeSats. The first flight, with a single 3U CubeSat, CLICK-A will demonstrate a >10 Mbps downlink. On the second flight, with two identical 3U CubeSats, CLICK-B/C, a >20 Mbps crosslink will be demonstrated in addition to downlinks.
In this paper representative link budgets for the crosslink are presented, including both communications and beacon lasers. The payload Pointing, Acquisition and Tracking (PAT) system is introduced, and the performance of the second stage closed loop tracking signal processing is assessed. Errors below 1 μrad are reported from test and simulation. The communication detector of the payload is a 200 μm InGaAs Avalanche PhotoDetector (APD), with a 1 GHz bandwidth and a dynamic range of more than 40 dB provided by programmable gain amplifiers. The APD performance enables a data rate of 17.7 Mbps at a range of 520 km. The timing accuracy of the detector is better than 130 ps.

Introduction

The success and rapid development of CubeSats in the last decade have led to a record number of small satellites in low Earth orbit. As the number of CubeSats grow, so does their need for high-throughput communications and bandwidth in the radio frequency (RF) spectrum. Radio licensing, required due to the finite amount of bandwidth available, is a logistical challenge. The advent of CubeSats has the potential to enable swarms and distributed measurements on a large scale, creating a need for high precision positioning, navigation and timing systems. Free-space optical communications provide a high performance communication option, less constrained by spectral efficiency and without the difficulties of spectrum allocation, coordination, and licensing. Ranging and time transfer at optical frequencies have the potential for order of magnitude improvements over RF methods.

The Cubesat Laser Infrared CrosslinK (CLICK) mission's goal is to demonstrate miniaturized transceivers capable of full-duplex high rate optical communications and high precision ranging between two nanosatellites. CLICK is jointly developed by the Massachusetts Institute of Technology (MIT), the University of Florida (UF), and the NASA Ames Research Center. The mission plan includes two separate launches of a total of three 3U CubeSats. In the first flight, the CLICK-A CubeSat will demon-

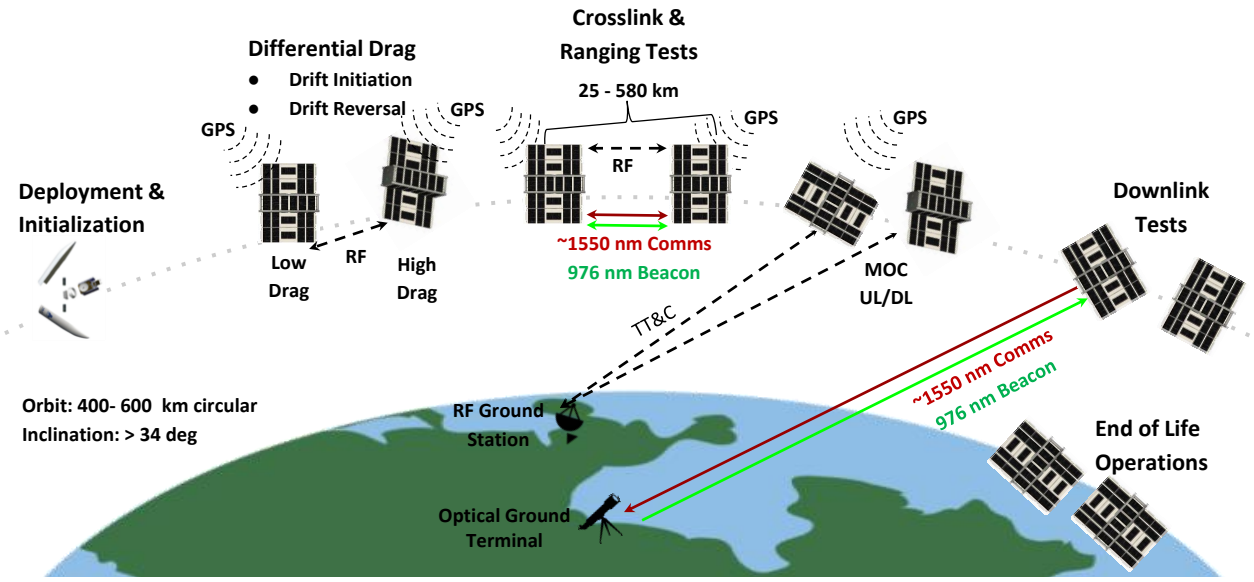

Figure 1: Concept of operations for the CLICK-B/C mission.

strate a >10 Mbps downlink to the Portable Telescope for Laser communications (PorTeL), which is further described in *Riesing*[1] and *Riesing et al.*[2] The payload for CLICK-A was initially developed as MIT's Nanosatellite Optical Downlink Experiment (NODE), and is further described in *Clements et al.*[3] and *Payne et al.*[4] In the second flight, two 3U CubeSats, CLICK-B & -C, will demonstrate a full-duplex crosslink, over separations from 25 km to 580 km. The spacecraft will also demonstrate a downlink to PorTeL. The extended goal is to reach crosslink data rates up to 50 Mbps and a timing accuracy better than 200 ps. This paper will focus on the CLICK-B/C mission and the prototype development effort for the pointing system and the receive detector.

CLICK Mission

Concept of Operations

The Concept of Operations for the CLICK-B/C flight is shown in fig. 1. The two spacecraft will be deployed in a string of pearls configuration in low Earth orbit, at an altitude from 400-600 km, and with an inclination greater than 30 degrees. Upon deployment and commissioning, the two spacecraft will use differential drag to begin a relative drift to the short distance test range of 25 km over the course of approximately 7 days. The drift will continue to be managed as the spacecraft further separate to the long distance test range of 580 km over an additional 2-3 weeks. At the 580 km boundary of the test range, the relative drift will be arrested and reversed to repeatedly traverse the test range over the remainder of the 6-12 month mission lifetime. While operating, the satellites will periodically share orbital state information via a low-rate radio crosslink. This information is used for drag management as well as the initial acquisition step of the pointing, acquisition, and tracking (PAT) sequence. Following crosslink experiments, telemetry and test results are downlinked via radio. The terminal optical layout is shown in fig. 2.

The payloads use a Master Oscillator Power Amplifier (MOPA) scheme to transmit. The 200 mW average power, 14.6 arcsec FWHM communications laser is set to 1537 nm for CLICK-B and 1563 nm for CLICK-C to enable spectral isolation during duplex operation. This isolation is implemented via a 45 degree angle of incidence dichroic filter that is placed at the output of the transmit collimator as shown in fig. 2. The filter reflects the transmitted signal while passing the received signal to the Avalanche Photo-Diode (APD) detector, which is equipped with two bandpass filters. These filters have a combined optical density of 10 to further reduce effects of stray

Link Parameter	APD		Quadcell		Camera	
P_{Tx} (dBW)	-6.99	200 mW avg.	-6.02	250 mW avg.	-6.02	250 mW avg.
G_{Tx} (dB)	93.45	120.2 μrad $1/e^2$	48.11	22.2 mrad $1/e^2$	48.11	22.2 mrad $1/e^2$
G_{Rx} (dB)	96.17	⌀20 mm Aper.	96.17	⌀20 mm Aper.	94.28	⌀16.1 mm Aper.
L_{path} (dB)	-253.45	580 km	-257.46	580 km	-257.46	580 km
L_{ptg} (dB)	-2.30	9.07 μrad (1σ)	-1.84	1.5 mrad (1σ)	-1.84	1.5 mrad (1σ)
$L_{\mathrm{Tx,imp}}$ (dB)	-1.55	est.	-1.02	est.	-1.02	est.
$L_{\mathrm{Rx,imp}}$ (dB)	-0.86	est.	-1.15	est.	-1.10	est.
P_{Rx} (dBW)	-79.53	avg.	-123.21	avg.	-125.06	avg.
$P_{\mathrm{Rx,bkgd}}$ (dBW)	<-157	non-eclipse	<-152	non-eclipse	<-144	non-eclipse
SNR_e (dB)	10.4	est.	12.2	est.	13.1	est.
Additional Notes: 1550 nm Tx, 976 nm Beacon, SNR_e is electrical signal-to-noise ratio						

Table 1: Crosslink Link Budgets

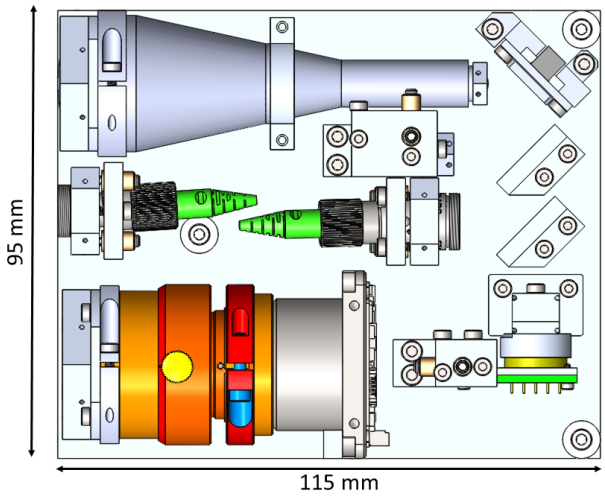

Figure 2: CLICK-B/C Optical Layout

light and optical background in the field of view.[5] The communications data is encoded with Pulse-Position Modulation (PPM), with a pulse duration of 10 ns. The number of symbols can vary between 4 and 128 per pulse. The received data is decoded via one of two implemented receiver architectures: 1) an Analog to Digital Converter (ADC) with a matched filter; 2) a Time to Digital Converter (TDC). The APD detector electronics and the TDC decoder are presented in this paper.

Link Budget

Three link budgets have been established to design and size the optical systems of CLICK-B/C. The first covers the link between the transmit laser and the APD, the second is the beacon laser to the quadcell, and the third addresses the beacon laser to the camera, and in all three for a crosslink of 580 km. The various losses and parameters, along with the estimated Signal-to-Noise Ratio (SNR), can be found in table 1. P_{Tx} is the average power transmitted by each laser. G_{Tx} is the transmit aperture gain, and G_{Rx} is the receive aperture gain. L_{path} is the path loss, and L_{ptg} the pointing loss. $L_{\mathrm{Tx,imp}}$ and $L_{\mathrm{Rx,imp}}$ are the losses due to the optical system, at the the transmitter and at the receiver, including dichroic filters, fiber connectors, and reflections. The end result is the received P_{Rx}. The received background power, $P_{\mathrm{Rx,bkgd}}$, includes background starlight in the field of view and stray light outside the FOV from the sun (non-eclipse) or moon (eclipse) and earth is included. To obtain the electrical signal-to-noise ratio, SNR_e, several noise and bias sources are taken into account. For instance, camera and quadcell sensor dark current and read noise is included with the received background, and the APD detector model includes 1550 nm crosstalk.

Pointing, Acquisition and Tracking

A Micro-Electro-Mechanical System (MEMS) Fine Steering Mirror (FSM) placed at the exit pupil of the Keplerian telescope enables Vernier steering of the transmit laser via the Fine PAT System (FPS). The PAT system employs a 500 mW, 976 nm beacon laser with a 0.75 deg FWHM beam divergence, which is separate from the communications laser and is mounted in the central aperture shown in fig. 2. The PorTeL optical ground station is also equipped with a 976 nm beacon laser. The beacon beam is fixed with respect to the structure and is steered using spacecraft body pointing via the Coarse PAT System (CPS). The open-loop coarse acquisition is achieved via the radio-relayed GPS-based orbit information. The closed-loop coarse

tracking is achieved via measurements of the beacon signal using a camera equipped with an Aptina MT9P031 silicon CMOS detector and a COTS lens assembly. The FPS also utilizes the beacon signal, which is simultaneously received by the telescope and routed onto a silicon quadrant PIN detector (quadcell) via an additional dichroic filter.

Fine PAT System

This subsection describes the FPS feedback loop from the quadcell to the FSM in detail.

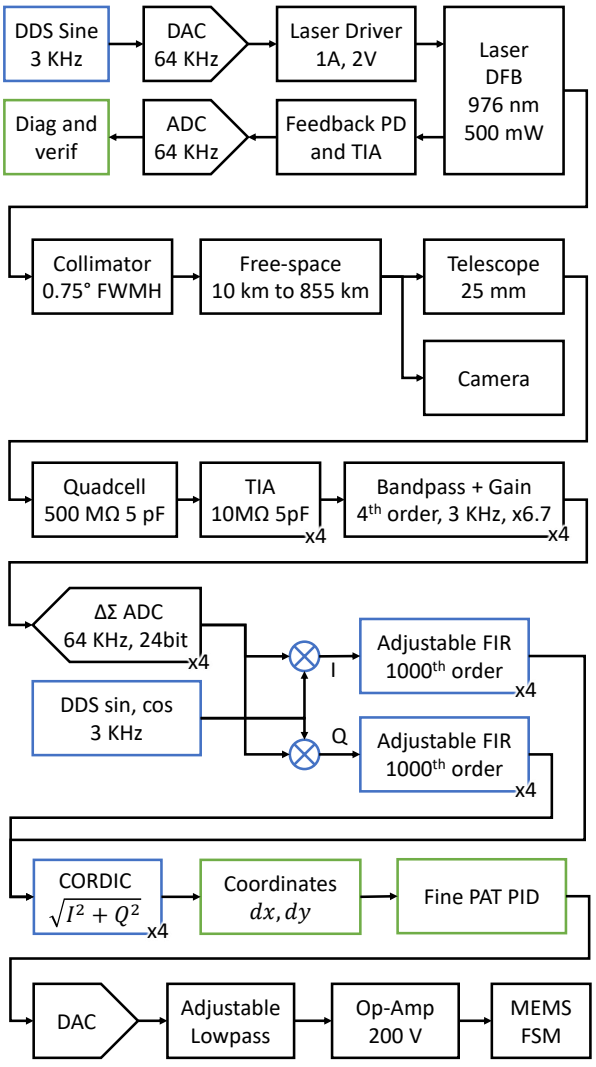

Figure 3: Signal flow through the second-stage PAT system. Blocks implemented in the FPGA Fabric are colored in blue, block on the FPGA micro-controller are in green.

Figure 3 describes the FPS signal flow from one spacecraft to the other. Each spacecraft modulates its beacon laser with a 3 kHz sine wave using a low-speed Digital to Analog Converter (DAC). A monitoring photodetector is used with an ADC to maintain a stable beacon laser power and to detect beacon malfunctions. The light is sent through a fiber to a collimator, and is emitted towards the other spacecraft. The 10X magnification of the payload receiving telescope gives the quadcell detector a larger geometric light collection area, as well as multiplying the measured angle by 10, boosting sensitivity to pointing error. This detector is operated in photovoltaic mode in order to reduce the noise as much as possible. The quadcell is followed by a 10 MΩ Trans-Impedance Amplifier (TIA), with a gain optimized to retain as much dynamic range as possible to enable free-space ranges from 10 km to 800 km. After the TIA, an operational amplifier-based bandpass filter serves as a second-stage coarse filtering with some extra gain. The signal is then digitized by a 24-bit, 4-channel simultaneous sampling delta-sigma ADC. The signal is transmitted to the payload FPGA, where 4 parallel homodyne demodulators recover the amplitude of the 3 kHz sine modulated beacon. The demodulators are each built around a 1000 tap Finite Impulse Response (FIR) filter. The frequency response of the FIR based filters have been tested and can be seen in fig. 4.

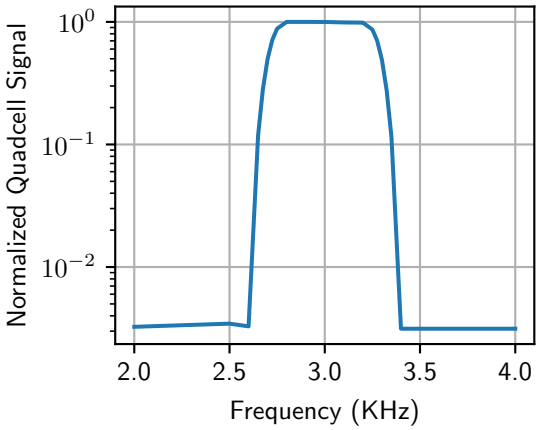

Figure 4: Quadcell and filter frequency response.

Using Digital Signal Processing for demodulation has several advantages. The low frequency noise sources are entirely eliminated, including the flicker noise from amplifiers and high impedance TIA errors such as current leakage. The large FPGA resources available in the CLICK-B/C payload allows

high order, steep filters to be built with good flatness. These filters can be adapted to support the dynamic ranges required by the crosslink operations. Finally, the bandwidth of the detector can be tuned with precision. The required bandwidth for the FPS depends on the host spacecraft Attitude Determination and Control System (ADCS) performance. The performance is difficult to predict for low cost spacecraft like CubeSats, and a body-pointed optical system like the CLICK payload imposes a dynamic mode of operation for the ADCS system, like slewing to target a ground station from low-Earth orbit. DSP algorithms allow filtering with a stable central frequency, using a precise clock as a reference. Since pointing residuals of high quality ADCS may be significant only at frequencies as low as 10 Hz in some use cases, very narrow band-pass filters are desirable.

Once the In-phase (I) and quadrature (Q) components of the signal have been computed, the amplitude and phase of the four signals are calculated using the COordinate Rotation DIgital Computer (CORDIC) algorithm. The ADC and the FIR filters run at a sampling rate of 64 kHz, the filters and the CORDIC engine use an internal of 64 MHz to reuse FPGA hardware resources as much as possible. The amplitude of each quadrant is used to compute the x and y coordinate of the spot on the quadcell. The phase of the incoming beacon is also calculated, and can be used as a very low rate (200 bps to 10 bps) communication channel for handshakes, protocol, data rate negotiation, and identification. With the x and y quadcell coordinates as an error input, a PID controller is used to drive the FSM to center the beam on the quadcell. The FSM is driven using a 16-bit DAC followed by a tunable lowpass filter and high-voltage amplifiers, closing the fine PAT loop.

Fine PAT Verification Setup

A test setup has been assembled in order to validate the functionality of the fine PAT system and assess its performance,[6] seen in fig. 5. The 976 nm laser source is identical to the flight version. An initial FSM is used to inject an angle disturbance. A second FSM is controlled by the PID controller and is used to close the fine PAT loop. The second FSM and its control circuit are representative of the current flight design. The beam goes through a 50:50 beamsplitter, half of the beam is directed to a camera, and used as a reference to measure the incidence angle. The other half of the beam travels to a second 50:50 beam-splitter which directs half the signal to a power meter, and the other half to a quadcell. The quadcell

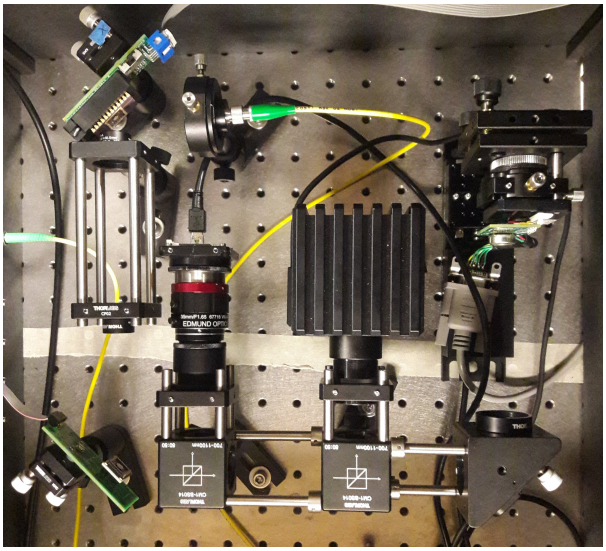

Figure 5: Picture of the second-stage PAT validation setup

used on this setup differs from the payload design as its trans-impedance gain is only 10 kΩ, 1000 times less than required, and it also lacks the second-stage analog coarse bandpass filter. The quadcell layout itself is also different, with a larger gap between the quadrants. The ADC and the FPGA however, are identical to the payload design.

Breadboard Quadcell Performance

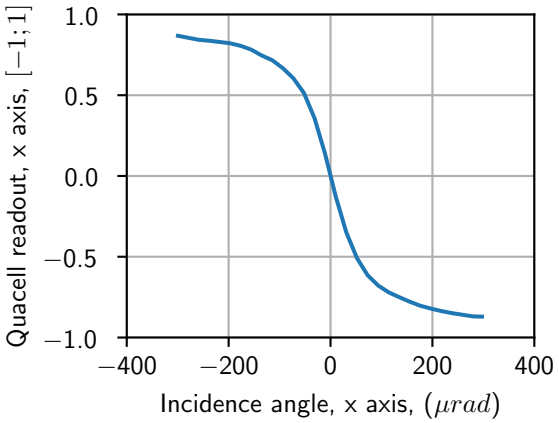

Figure 6: Quadcell transfer function along the x axis, from the incidence angle on the payload to quadcell coordinates.

The transfer function of the quadcell and the DSP

algorithms have been measured using the test bench. The transfer function is plotted in fig. 6, and a close-up view of the center of quadcell is shown in fig. 7.

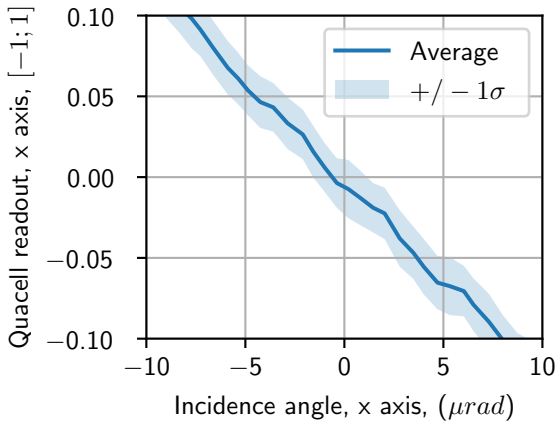

Figure 7: Quadcell transfer function near the quadcell center.

The measurements of figs. 6 and 7 were obtained with a beam of 100 nW, corresponding to closing the loop at a range of close to 6 km. The bandwidth was set to 200 Hz. The noise of the quadcell incidence angle measurement is below $1\sigma = 1\mu$rad with this configuration, which is the required accuracy in order to close the fine PAT loop. In order to meet the noise requirement at the desired range of 580 km, the SNR needs to be improved by a factor of 4500.

Modulation and Demodulation

After a successful acquisition by the PAT system, the payload transmitter and one of the payload receiver systems will be turned on. The structure of the payload optical modem is shown in fig. 8. The ADC and TDC receiver systems share a common transmitter, which uses a wavelength-to-amplitude modulation scheme. Both receivers also share a common APD detector and gain control circuit, where each receiver can be selected using an RF switch.

Wavelength-Amplitude Modulation Transmitter

The seed laser used by the CLICK-B/C payload is similar to that used by *Clements et al.*[3] in the NODE design. The transmitter uses a laser diode, and its wavelength is slightly adjustable via change in the bias current or change in temperature with a Thermo-Electric Cooler (TEC). A modulated signal from the FPGA is applied to the laser diode via an AC-coupled input to the bias current. The diode's output is the sum of the DC bias current and the coupled modulation signal. The extinction ratio, defined as the ratio of optical power for a PPM pulse generated by the coupled FPGA signal to a empty time slot at the DC current level, is low and close to 1. However, the induced variation in the diode current also changes the output wavelength in the form of a proportional laser frequency chirp. The light from the diode is directed to a narrow band Fiber Bragg Grating (FBG) through a circulator. Wavelengths within the FBG band, corresponding to an induced shift in current by the FPGA (a PPM pulse), are reflected back into the circulator. Wavelengths outside the FBG band corresponding to the DC current level (an empty PPM time slot), are transmitted through the FBG and absorbed by an attenuator and a photodetector. This greatly increases the extinction ratio to more than 30 dB. After the extinction filter, the seed laser light is passed to the EDFA.

Three PIN photodiodes are used to sense the optical power before and after the extinction filter, as well as the optical power rejected by the filter. The measurements from these detectors are used with a feedback system to adjust the DC bias current and the temperature of the laser to keep its wavelength just outside the the FBG band, within easy reach of the modulated wavelength shift. The design of the transmitter has been improved over that used for NODE, as now the modulation signal is generated by a FPGA Serialization-Deserialization (SERDES) module, allowing the optical output to be modulated on and off with a resolution as low as 400 ps. A Programmable Gain Amplifier (PGA) has been inserted to adjust the depth of modulation of the electrical signal, adding another way to adjust the wavelength deviation of the seed laser diode to stay within the band of the extinction filter.

Communication Detector

The board driving and supporting the Avalanche Photodetector (APD) for the CLICK mission is based on previous projects, such as the CHOMPTT CubeSat mission and the MOCT demonstration.[7] The APD is a free-space Voxtel InGaAs APD in a 15 mm diameter package, and has a 1 GHz bandwidth. Two PGAs in series amplify the differential signal from the APD and drive the board's differential output. The reverse bias applied to the APD is driven by a high voltage DC-DC boost converter (HVBC), which can be set dynamically with a DAC

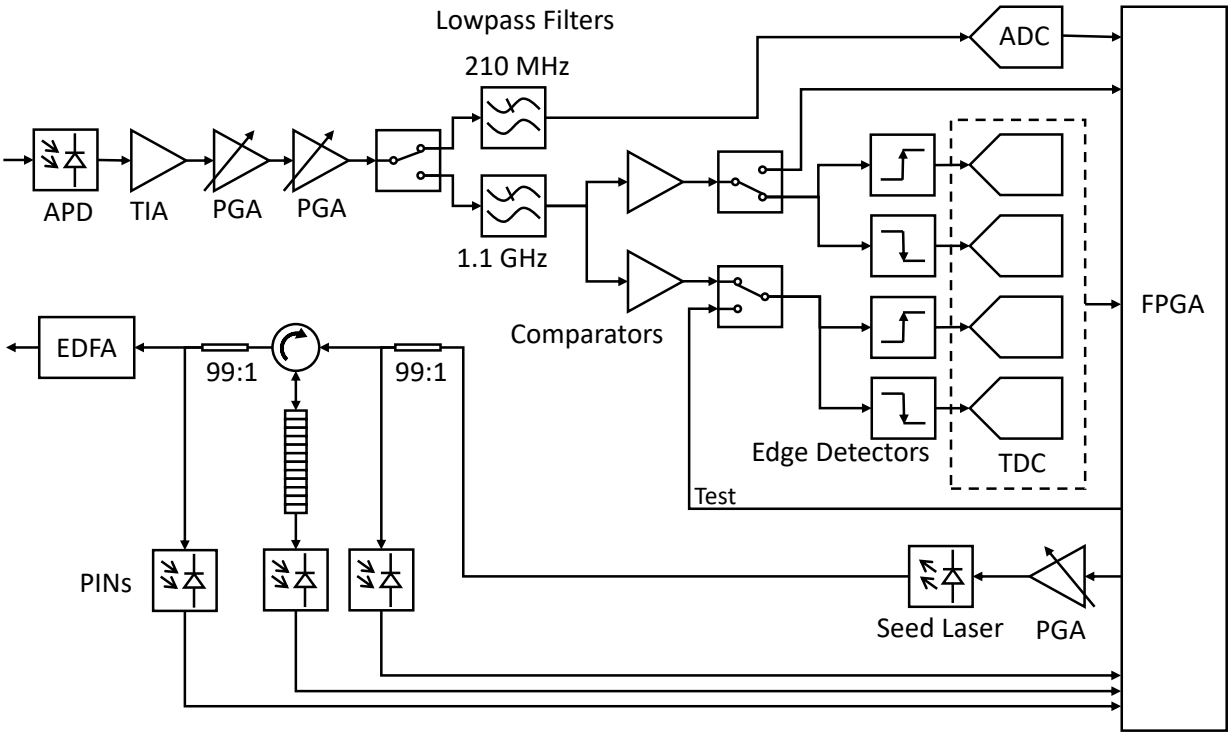

Figure 8: Block diagram of the modulator and demodulator hardware

over a serial connection. The reverse bias voltage and current draw through the APD are monitored and made available over the serial connection with a logarithmic amplifier and an ADC, along with a reading of the temperature beneath the APD. A TEC controller on board may be used in conjunction with the temperature sensor to provide active thermal control via the TEC contained inside the APD housing. Images of the flatsat version of the new detector board, named the Near-IR Optical detector with Variable Amplification (NOVA) board, are shown in fig. 9 both with and without (figs. 9a and 9b) its aluminum frontplate. The frontplate is designed to not only provide a thermal sink for the APD itself, but also to separate the noise aggressors and receptors on the board with a physical, electrically grounded barrier. This flatsat version of the board was made with testing in mind; there are several test points, as well as mounting points, which support 1/4-20 inch screws as well as a 30 mm cage system.

The APD is operated with a gain M of 40. The APD package includes a TIA with a gain of $R_{\mathrm{TIA}} = 2.75\ \mathrm{k}\Omega$. With the APD responsivity $Q_{1550} = 1.05$ A/W, the APD output can be calculated from the incoming optical power P_{Opt} with eq. (1).

$$V_{\mathrm{APD}} = P_{\mathrm{Opt}} \cdot Q_{1550} \cdot M \cdot R_{\mathrm{TIA}}, \tag{1}$$

where V_{APD} is the voltage signal measured from the APD output.

The two Programmable Gain Amplifiers (PGA) following the APD each have an adjustable gain ranging from -6 dB to 26 dB. Since the physical distance between the first and the second PGA is small, the output of the first has not been matched to the input of the second in order to preserve gain. This introduced a factor of 100 Ω/120 Ω due to the 10 Ω resistor integrated in the output of the PGAs, and the PGAs internal terminations of 100 Ω. The output V_{board} of the receiver board can be obtained with eq. (2).

$$V_{\mathrm{board}} = \frac{100\ \Omega}{120\ \Omega} \cdot V_{\mathrm{APD}} \cdot \sqrt{10^{\frac{G_{\mathrm{PGA1}}+G_{\mathrm{PGA2}}}{10}}} \tag{2}$$

Figure 10 shows a typical pulse obtained with the first prototype of the receiver, obtained by averaging the board output over many samples. The negative section of the curve and the under-damped oscillations after the pulse are anomalies, indicating an error in the design of the low-pass filter included on the board.

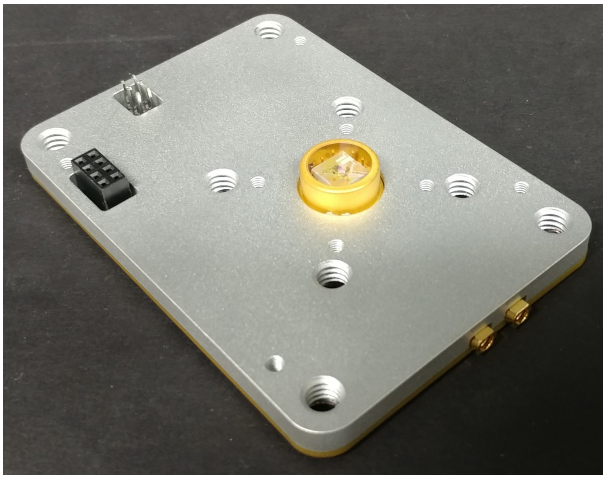

(a) With Aluminum shield

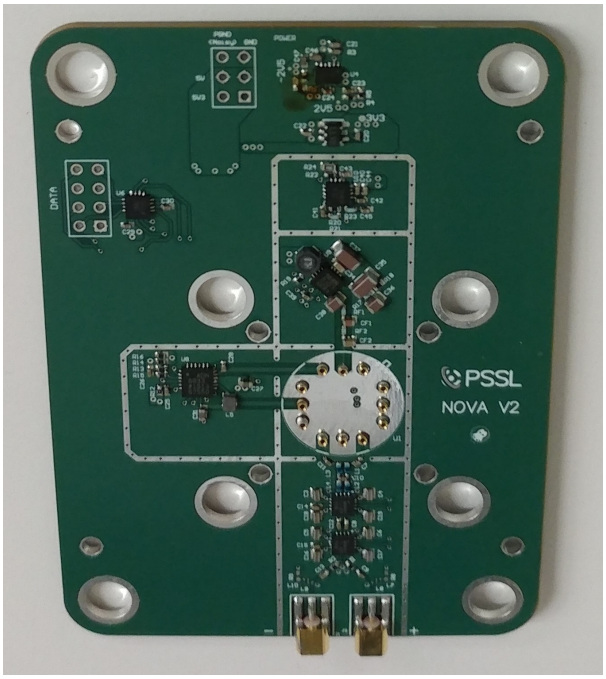

(b) Uncovered

Figure 9: NOVA detector board, flatsat version.

In order to characterize the detector board for use with the ADC and matched filter receiver, the SNR has been measured over a range of optical power levels. The results are plotted in fig. 11, along with the theoretical SNR based on the APD noise equivalent power and the PGA voltage noise. Automatic gain control has also been factored into the theoretical curve. The optical power has been mapped to the communication range using the link budget results. The first prototype is nearly capable of closing the link at the required distance of 580 km with a

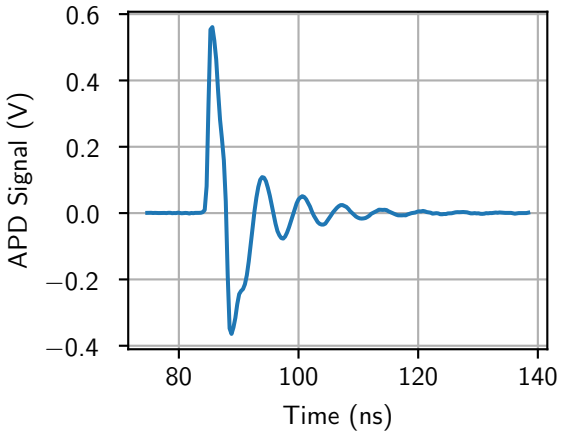

Figure 10: A pulse from the APD detector. Note that modification to the low pass filter design should address ringing anomalies.

PPM order of 32, allowing a data rate of 17.7 Mpbs. The measured SNR is 4 times lower than the predicted values, this is partly attributed to the filtering anomalies mentioned above, and to unaccounted-for optical losses between the power meter and the APD.

Time-to-Digital Receiver

Each payload includes an ams TDC-GPX2 Time-to-Digital Converter (TDC) as one of its receiver systems, alongside the ADC. The system can be seen in fig. 8. The TDC receiver system can be selected using the APD signal multiplexer. The signal is first directed through a through a 1.1 GHz low pass filter to reduce high-frequency out-of-band noise. After the filter, the signal is split and sent to one of two pairs of adjustable threshold edge detectors. These detectors allow for the pulse to be sampled at four points, twice on the rising edge at two different thresholds, and twice at the falling edge at those same thresholds. These four signals are then sent to each of the four TDC channels, each recording an independent time offset from the spacecraft's reference clock for each event, with a resolution of around 20 ps.

The TDC transmits the time-offset data of measured events from each of its channels to the FPGA, which combines the measurements and generates a timestamp for the detected pulse. These timestamps can then be used in PPM demodulation to receive data at up to 50 Mbps, to calculate range down to 10 cm, and for precision time transfer with <200 ps

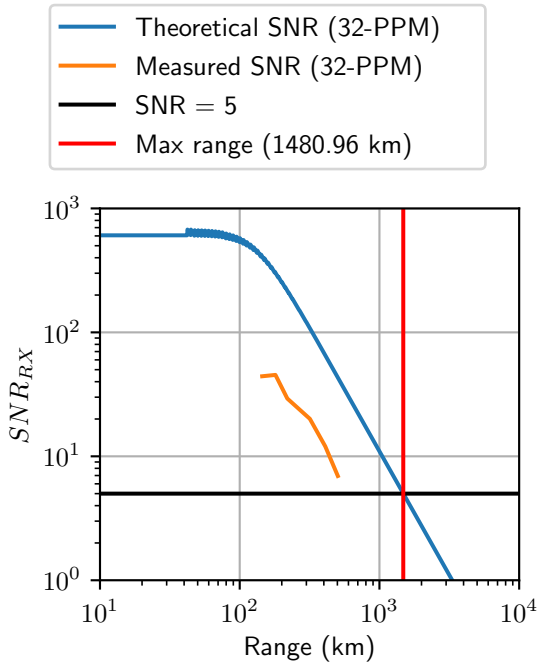

Figure 11: Signal to Noise Ratio of the APD and the amplifier chain as a function of range. The maximum theoretical range is 1480 km in 32-PPM, while the measured maximum is 520 km on the first prototype.

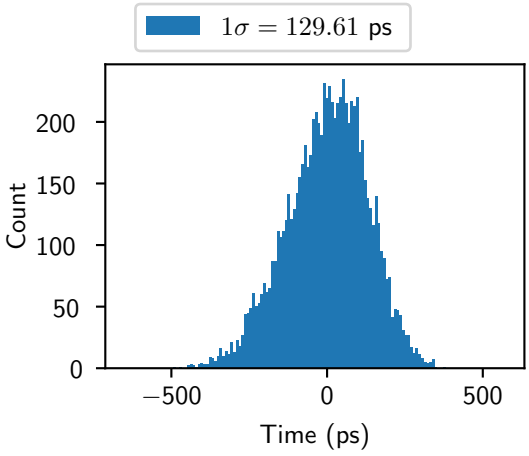

Figure 12: Rising edge time error (jitter).

resolution. This is in line with the timing error of the APD receiver, plotted in fig. 12. As these calculations can be performed in parallel using the available FPGA resources, with careful data modulation schemes, they can all be made simultaneously.

Conclusion

The CLICK mission will demonstrate high data rate optical communications along with precision ranging and time transfer. The CLICK-B/C flight will demonstrate crosslinks, uplinks and downlinks in low earth orbit. Link budget analysis has been performed, and links over ranges greater than 580 km are supported by the CLICK design.

The second stage pointing, acquisition and tracking loop functionality has been tested, and its digital signal processing has been validated. The fine PAT design can be tuned for the spacecraft pointing performance while maintaining a large dynamic range. The tracking error is below 1 μrad. A more representative version of the quadcell and its analog circuitry is required to achieve the required range. Future work on the fine PAT will focus on improving and reducing the noise of the quadcell readout circuit and on characterizing the ability of the PID controller to reject disturbances.

The avalanche photodetector used by the receivers has been evaluated. The APD noise performance is close to the desired specifications. With higher PPM modulation orders, the link can be closed beyond our target range of 580 km. An anomaly has been found in the APD response, requiring a modification of its filter. The jitter performance meets the requirements for precision time transfer. Future work for the APD detector boards includes responsivity testing and forming the relationship between the logarithmic amplifier output and average received optical power.

The integration of the various electronic components into an Engineering Design Unit (EDU) is in progress. CLICK-B/C is targeting a launch in the 2020-2021 timeframe.

References

[1] Kathleen Michelle Riesing. *Portable Optical Ground Stations for Satellite Communication.* PhD thesis, 2018.

[2] Kathleen Riesing, Hyosang Yoon, and Kerri Cahoy. A portable optical ground station for low-earth orbit satellite communications. *2017 IEEE International Conference on Space Optical Systems and Applications, ICSOS 2017*, (Llcd):108–114, 2018.

[3] Emily Clements, Raichelle Aniceto, Derek Barnes, David Caplan, James Clark, Iñigo del Portillo, Christian Haughwout, Maxim Khatsenko, Ryan Kingsbury, Myron Lee, Rachel Morgan, Jonathan Twichell, Kathleen Riesing, Hyosang Yoon, Caleb Ziegler, and Kerri Cahoy. Nanosatellite optical downlink experiment: design, simulation, and prototyping. *Optical Engineering*, 55(11):111610, September 2016.

[4] Cadence Payne, Alexa Aguilar, Derek Barnes, Rodrigo Diez, Joseph Kusters, Peter Grenfell, Raichelle Aniceto, Chloe Sackier, Gregory Allan, and Kerri Cahoy. Integration and Testing of the Nanosatellite Optical Downlink Experiment. Technical report.

[5] Laura Yenchesky, Peter Grenfell, Mia LaRocca, and Kerri Cahoy. Optomechanical design for CubeSat laser infrared crosslinks. In *AIAA Scitech 2019 Forum*. American Institute of Aeronautics and Astronautics, January 2019.

[6] Ondrej Čierny and Kerri L. Cahoy. On-orbit beam pointing calibration for nanosatellite laser communications. *Optical Engineering*, 58(04):1, November 2018.

[7] Nathan S. Barnwell, Samantha Parry, Tyler Ritz, Paul Serra, and John Conklin. Laser amplifier system in a deep space optical transmitter for small satellites. In *AIAA SPACE and Astronautics Forum and Exposition*. American Institute of Aeronautics and Astronautics, September 2017.